



Research paper

Bio-inspired assembly of cubane-adjustable polyoxometalate-based high-nuclear nickel clusters for visible light-driven hydrogen evolution



Xin-Bao Han^{a,b}, Chao Qin^a, Xin-Long Wang^{a,*}, Yuan-Zhi Tan^b, Xin-Jing Zhao^b, En-Bo Wang^{a,*}

^a Key Laboratory of Polyoxometalate Science of the Ministry of Education, Faculty of Chemistry, Northeast Normal University, Changchun, Jilin 130024, PR China

^b State Key Laboratory for Physical Chemistry of Solid Surfaces, and Department of Chemistry, College of Chemistry and Chemical Engineering, Xiamen University, Xiamen, 361005, PR China

ARTICLE INFO

Article history:

Received 18 February 2017

Received in revised form 11 April 2017

Accepted 21 April 2017

Available online 24 April 2017

Keywords:

Polyoxometalate

Nickel

Cubane

Photocatalysis

Hydrogen evolution

ABSTRACT

By artificial mimic of the natural [FeFe]-hydrogenases, a series of polyoxometalate-based high-nuclear Ni clusters containing a varying number of $\{Ni_4O_4\}$ cubane cores, $K_{1.5}Na_{26.5}\{Ni_4(OH)_3(PO_4)_4(A-PW_9O_{34})_4\} \cdot 62H_2O$ (**1**), $Na_{28}\{Ni_4(OH)_3(PO_4)_4(A-PW_9O_{34})_2(B-PW_9O_{34})_2\} \cdot 102H_2O$ (**2**), and $Na_{28}\{Ni_4(OH)_3(VO_4)_4(B-PW_9O_{34})_4\} \cdot 74H_2O$ (**3**), were synthesized and systematically characterized. Compounds **1**–**3** contain $\{Ni_{16}(XO_4)_4(OH)_{12}\}$ ($X = P, V$) core encapsulated by the trivacant A-/B-/ $\{PW_9O_{34}\}$ ligands. Compounds **1**–**3** as homogeneous catalysts for visible-light-driven H₂ evolution indicate that they not only show high photocatalytic performance (High TON of 578.8, 679.1, and 931.1 for **1**–**3** were achieved, respectively), but also their catalytic performance was improved with the increasing number of $\{Ni_4O_4\}$ cubanes. Multiple stability experiments confirm that compounds **1**–**3** maintain their structure intact under the photocatalytic conditions. The above research provides a platform for mimicking the structures of natural hydrogenases to further explore more efficient and inexpensive H₂ evolution catalysts.

© 2017 Published by Elsevier B.V.

1. Introduction

Hydrogen production from artificial photosynthesis (AP) is an intriguing approach to storing and converting solar energy into renewable and non-fossil-based fuels [1–9]. The exploration of H₂ evolution catalysts (HECs) to satisfy the requirements of the commercial application is currently a formidable yet exceedingly engaging challenge. As more and more biological functions of the cubane-like [Fe₄S₄] cluster in natural photosystem I (PSI) were discovered, biomimetic chemistry of [Fe₄S₄] and related clusters has become an important subject [10–14]. Such biomimetic molecular clusters i) are based on earth-abundant elements, which holds great potential for large-scale commercial application, ii) have well-defined composition and molecular structures allowing the exploration of structure–property relationship and mechanistic

features of the catalytic H₂ evolution reactions (HERs), and iii) may help tune H₂ evolution performance at the molecular level. Their unique advantages offer breakthrough points for constructing highly efficient and well-defined molecular HECs.

Polyoxometalates (POMs) is a sub family of soluble anionic metal-oxo clusters constituted by W, Mo, V, Nb, or Ta ions in high oxidation states [15–19]. They possess oxygen-rich surfaces and proved to be ideal inorganic building blocks for targeting transition metal (TM) cubane clusters [20–26], as elucidated in a recent review of our group [27]. What's more important is that the introduction of TM into POMs could help tune the band gap structures and even broaden the spectrum absorption of such molecular clusters from UV to the visible-light region, thereby providing the possibility for the synthesis of visible-light-driven POM-based HECs.

In an effort to develop more efficient, more viable, and low-cost molecular catalysts to realize the widespread use of solar energy, we have been focused on designing and synthesizing $\{M_4O_4\}$ cubane and/or $\{M_3O_4\}$ quasi-cubane core-containing photocatalysts to mimic the natural photosystem (PS). At the outset of our work, we have mimicked the oxygen-evolving complex (OEC)

* Corresponding authors.

E-mail addresses: wangxl824@nenu.edu.cn (X.-L. Wang), wangeb889@nenu.edu.cn (E.-B. Wang).

$\{Mn_4O_5Ca\}$ of PSII and successfully prepared a series of POM-based water oxidation catalysts (WOCs) [21,22]. Given that the “footprint” of $\{M_4O_4\}$ cubane core is very close to the natural $[Fe_4S_4]$ cubane cluster of $[FeFe]$ -hydrogenases, as an extension of our work, we intend to take a step further to probe the generality of such biomimetic POM-based metal clusters as visible-light-driven HECs. However, we noticed that there is almost no relevant work for reference [28,29]. Only one Ni-cubane-encapsulating POM exhibits H_2 evolution activity under visible-light illumination hitherto [30], even though various types of polyoxotungstates with photocatalytic H_2 evolution activities under UV-light irradiation have already been reported [31–40]. It means that building POM-based TM-cubane clusters is a big challenge in current synthetic chemistry. As a consequence, in order to trace some instructive laws in this field, some key questions remain to be addressed: Which of the transition metal elements presents the optimal choice for POM-based HECs? How to synthesize TM cubane-containing POMs to achieve fine adjustment of the number of cubane? What is the relationship between the number of cubane and catalytic performance? If we could prepare a series of reliable structural paradigms, it may help shed light on these issues, and therefore, in the longer term, design and develop more efficient HECs with controlled active site and structure.

As we know, among the first-row TM elements, nickel is the ninth most abundant element in the Earth's crust [41]. It belongs to the same group as Pt on the periodic table, a best performing catalyst discovered to date for HER, but is much cheaper than Pt [3]. In nature, hydrogenase enzymes based on earth-abundant metals (nickel is one of them) can efficiently catalyze H_2 production with a turnover frequency (TOF) as high as 9000 s^{-1} [42,43]. Theoretical calculations show that Ni site of the hydrogenase plays an essential role in the hydrogen evolution reaction (HER) [44]. Given all that, Ni is a preferable choice for TM-substituted POM-based HECs. Meanwhile, it is noteworthy that subtle geometry variation of lacunary POMs enables their isomeric species to have different reactivity when coordination with TM metals. Hence, by ingenious use of the reactivity difference of isomeric forms of $\{PW_9O_{34}\}^{9-}$ toward TM metals, we now have succeeded in preparing three stable POM-based high-nuclear nickel clusters: $K_{1.5}Na_{26.5}[\{Ni_4(OH)_3(PO_4)\}_4(A-PW_9O_{34})_4] \cdot 62H_2O$ (**1**), $Na_{28}[\{Ni_4(OH)_3(PO_4)\}_4(A-PW_9O_{34})_2(B-PW_9O_{34})_2] \cdot 102H_2O$ (**2**), and $Na_{28}[\{Ni_4(OH)_3(VO_4)\}_4(B-PW_9O_{34})_4] \cdot 74H_2O$ (**3**). Compounds **1–3** contain a varying number of $\{Ni_4O_4\}$ cubane core (one, three, and five $\{Ni_4O_4\}$ cubane cores corresponding to **1**, **2**, **3**, respectively), reminiscent of the $[Fe_4S_4]$ cubane cluster of $[FeFe]$ -hydrogenases. Their successful preparation provides the possibility for systematical investigation on visible-light-driven H_2 evolution activities of POM-based complexes. Compounds **1–3** as the homogeneous catalysts for visible-light-driven H_2 evolution have been investigated in detail and high TON of 578.8 for **1**, 679.1 for **2**, and 931.1 for **3** were achieved, respectively. Further exploration of structure-performance relationship revealed that the catalytic activity improved with increasing number of $\{Ni_4O_4\}$ cubane. Furthermore, the reusability and stability of compounds **1–3** in the photocatalytic system were also examined in detail. We also carried out photophysical studies and initially put forward the HER mechanism of compounds **1–3**.

2. Results and discussion

2.1. Synthesis and structures of **1–3**

Directional synthesis of cubane-containing POMs is a significant challenge and commonly frustrated by the absence of a reliable synthetic strategy. It is well-known that lacunary derivatives of

POMs can be obtained by the removal of one or more $\{MO_6\}$ octahedra from their corresponding saturated species, which, in some cases, will result in positional isomers. It is the subtle variation of geometry that enables the isomeric species to have different reactivity. Two common trivacant isomers of Keggin ions, $A-\alpha-\{PW_9O_{34}\}^{9-}$ and $B-\alpha-\{PW_9O_{34}\}^{9-}$ are such cases. As shown in Fig. S1, the central PO_4 tetrahedron in $A-\alpha-\{PW_9O_{34}\}^{9-}$ is exposed at its base, whereas in $B-\alpha-\{PW_9O_{34}\}^{9-}$ it is exposed at its apex. This determines that $B-\alpha-\{PW_9O_{34}\}^{9-}$ is much easier to form cubane structure than $A-\alpha-\{PW_9O_{34}\}^{9-}$ when coordination with TM metals. So this raises a question if one can apply this difference to modulate the number of TM-cubanes. By use of different isomeric forms as reactive precursors, we have obtained a series of POM-based high-nuclear Ni clusters containing a varying number of $\{Ni_4O_4\}$ cubanes. Using A -typed isomer as starting materials without or with partial conversion from type A to type B , compounds **1** and **2** containing one and three cubane cores were synthesized respectively; only use of B -typed isomer compounds **3** containing five cubane cores were synthesized. This new method of using isomers of POMs to regulate the resulting structure opens a promising avenue for directional synthesis of POM-based complexes. In addition, several important synthetic factors should be emphasized. Firstly, the pH of reaction solution should be in the range 8.0–9.0. It is crucial for the assembly of compounds **1–3**. Beyond this pH range, negligible or no crystalline products were obtained in the same reaction system. Secondly, the reaction temperature plays an important role in synthesizing compounds **1–3**. Compound **1** was synthesized at room temperature. At a too high temperature, no target product is obtained. Compounds **2** and **3** were synthesized by refluxing the reaction solution because high temperature favors isomerization from type A to type B and favors bridging ligand $\{VO_4\}$ coordination with Ni^{2+} and $B-\alpha-\{PW_9O_{34}\}^{9-}$. Without refluxing, negligible or no crystalline products of compounds **2** and **3** were isolated. Thirdly, the presence of $\{PO_4\}$ or $\{VO_4\}$ is required to stabilize the hexadecanuclear-Ni clusters. We have also been devoted ourselves to synthesize a compound containing more than three $\{Ni_4O_4\}$ cubane units. Using $NiCl_2 \cdot 6H_2O$, $Na_8H[B-\alpha-PW_9O_{34}]$, and $Na_3PO_4 \cdot 12H_2O$ as the starting materials, we changed a lot of synthetic conditions. However, to our disappointed, we have not got aimed product. Considering the various coordination spheres of vanadium atom and similar bond length of V-O with P-O, $Na_3PO_4 \cdot 12H_2O$ was replaced by $NaVO_3$, and then compound **3** containing a central $\{Ni_4(VO_4)_4\}$ core encapsulated by four $\{(B-\alpha-PW_9O_{34})(NiOH)_3\}$ units was obtained, in which there are five $\{Ni_4O_4\}$ cubane units in all.

Compound **1** (Fig. 1c) contains a high-nuclearity nickel–phosphate cluster $\{Ni_{16}(PO_4)_4(OH)_{12}\}$ (**Ni16-1**) (Fig. 1b) and four $A-\alpha-\{PW_9O_{34}\}^{9-}$ units (Fig. 1a). The whole **Ni16-1** cluster is well encapsulated by four lacunary $A-\alpha-\{PW_9O_{34}\}$ POM units, allowing the nickel–phosphate cluster to be well isolated without terminal H_2O coordinating to the central nickel ions. From another point of view, compound **1** can be viewed as a tetramer comprising four tetra-nickel-substituted Keggin fragments $\{Ni_4(OH)_3(A-\alpha-PW_9O_{34})\}$ (Fig. 1d), connected with four $\{PO_4\}$ linkers (Fig. 1e). Alternatively, compound **1** can also be viewed as a central $\{Ni_4(PO_4)_4\}$ core (Fig. 1g) wrapped by four $\{(A-\alpha-PW_9O_{34})(NiOH)_3\}$ units (Fig. 1f) with idealized Td symmetry. Such a $\{Ni_4(PO_4)_4\}$ core comprises a central $\{Ni_4O_4\}$ cubane unit (Fig. 1h), which is structurally analogous to the $[Fe_4S_4]$ cubane. In the $\{Ni_4O_4\}$ cubane unit, the Ni–O distances are in the range $2.073(18)$ – $2.138(17)$ Å and the Ni···Ni distances range from $3.077(10)$ to $3.189(10)$ Å. It's noted that compound **1** is isostructural to recently reported $[\{Co_4(OH)_3(PO_4)\}_4(PW_9O_{34})_4]^{28-}$ [20,21].

Compound **2** crystallizes in the monoclinic space group C2/c. Compound **2** (Fig. 2d) consists of one central $\{Ni_{16}(PO_4)_4(OH)_{12}\}$ (**Ni16-2**) core (Fig. 2b), two lacunary $A-\alpha-\{PW_9O_{34}\}$ POM units

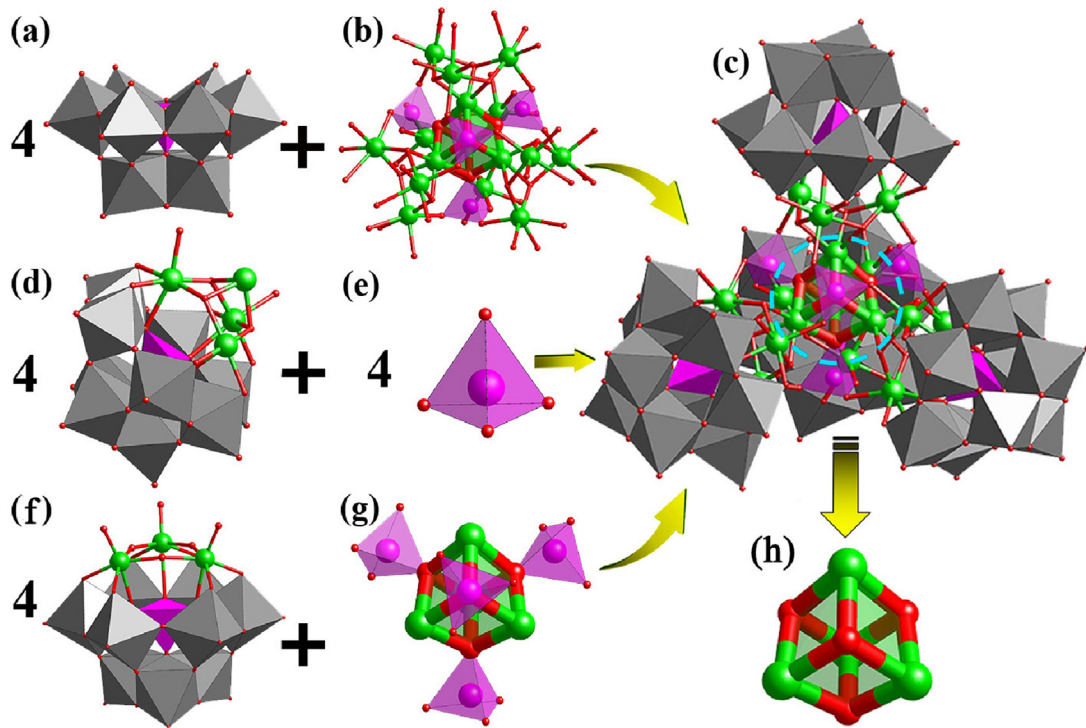


Fig. 1. Polyhedral and ball-and-stick representation of the various building blocks (a)–(g) of compound **1** (c); ball-and-stick representation of one $\{\text{Ni}_4\text{O}_4\}$ core (h) in **1**. WO_6 , gray octahedra; PO_4 , pink tetrahedra; O, red sphere; Ni, green sphere. (For interpretation of the references to colour in this figure legend, the reader is referred to the web version of this article.)

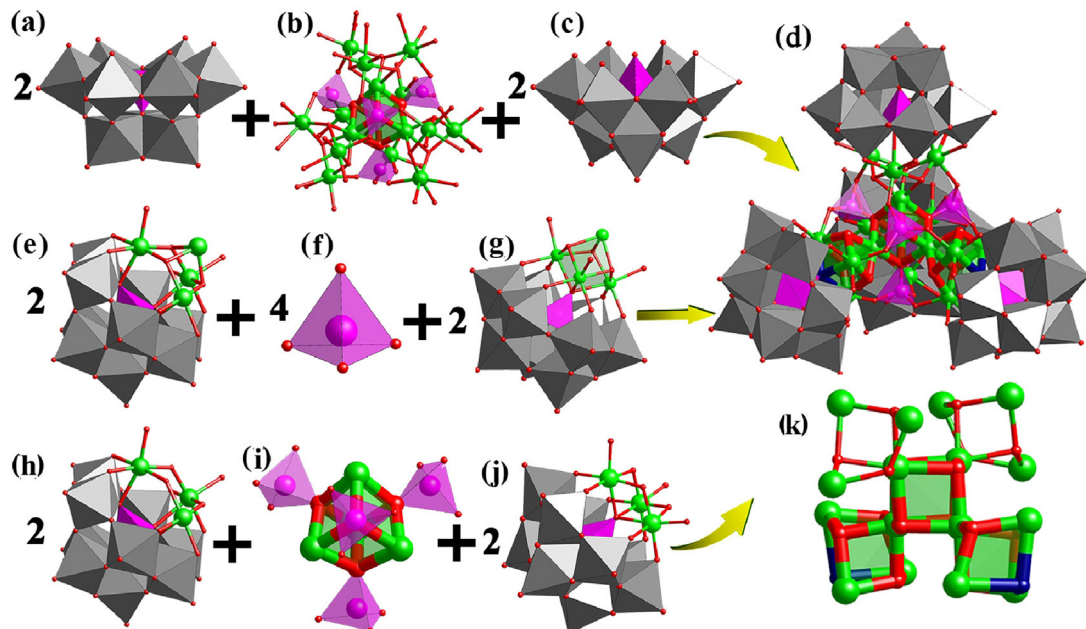


Fig. 2. Polyhedral and ball-and-stick representation of the various building blocks (a)–(j) of compound **2** (d); ball-and-stick representation of three $\{\text{Ni}_4\text{O}_4\}$ cubane cores (k) in **2**. WO_6 , gray octahedra; PO_4 , pink tetrahedra; O, red or blue spheres; Ni, green sphere. (For interpretation of the references to colour in this figure legend, the reader is referred to the web version of this article.)

(Fig. 2a), and two lacunary $B\text{-}\alpha\text{-}\{\text{PW}_9\text{O}_{34}\}$ POM units (Fig. 2c) with idealized T_d symmetry. The $\{\text{Ni16-2}\}$ core is structurally similar to the $\{\text{Ni16-1}\}$ core in compound **1**, but what is different is that the whole $\{\text{Ni16-2}\}$ cluster is encapsulated by two configurations of trivacant POM units, namely lacunary $A\text{-}\alpha\text{-}\{\text{PW}_9\text{O}_{34}\}$ POM unit and $B\text{-}\alpha\text{-}\{\text{PW}_9\text{O}_{34}\}$ POM unit. To our knowledge, such position isomeric clusters are very rare in POM chemistry. Like-

wise, the structure of compound **2** can be viewed as a tetramer of four tetra-nickel-substituted Keggin fragments (two $\{\text{Ni}_4(\text{OH})_3(A\text{-}\alpha\text{-}\{\text{PW}_9\text{O}_{34}\})\}$ (Fig. 2e) and two $\{\text{Ni}_4(\text{OH})_3(B\text{-}\alpha\text{-}\{\text{PW}_9\text{O}_{34}\})\}$) (Fig. 2g), which is further linked by four $\{\text{PO}_4\}$ linkers (Fig. 2f). In total, there are three $\{\text{Ni}_4\text{O}_4\}$ cubane units (Fig. 2k) in compound **2** owing to the partial conversion from $A\text{-}\alpha\text{-}\{\text{PW}_9\text{O}_{34}\}^{9-}$ to $B\text{-}\alpha\text{-}\{\text{PW}_9\text{O}_{34}\}^{9-}$. The $\{\text{Ni}_4\text{O}(\text{OH})_3\}$ unit in each $\{\text{Ni}_4(\text{OH})_3(B\text{-}\alpha\text{-}\{\text{PW}_9\text{O}_{34}\})\}$ unit also

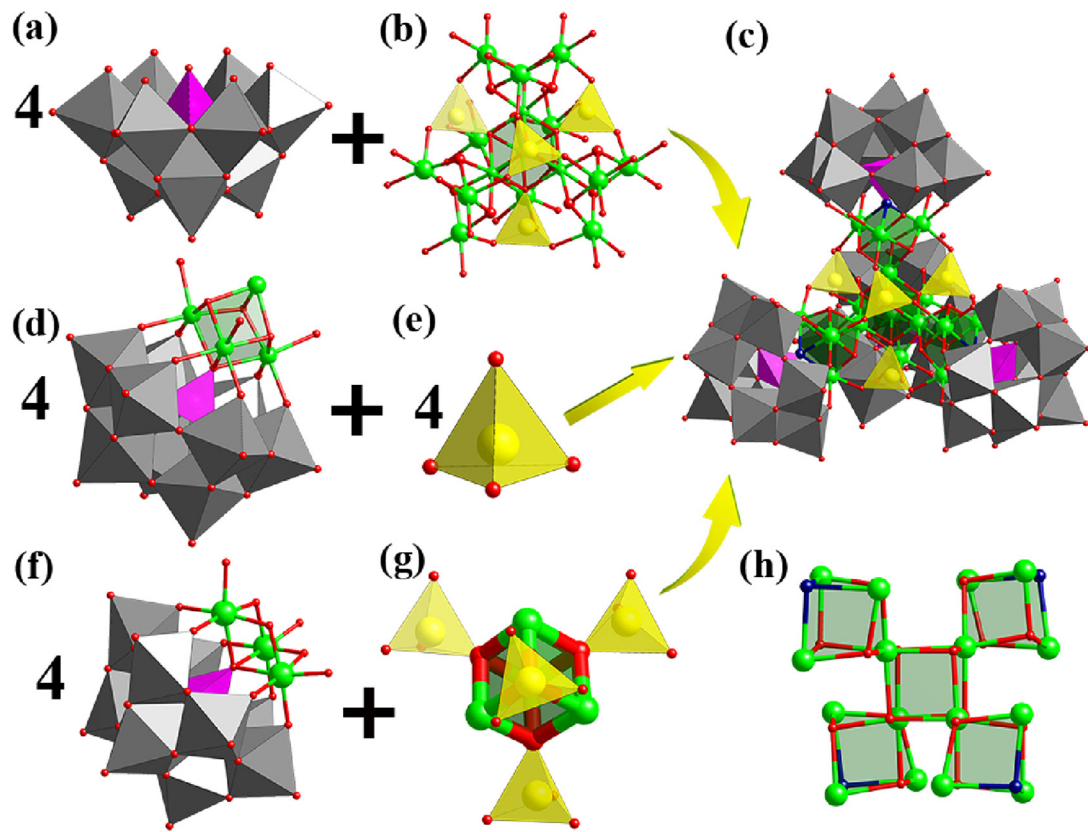


Fig. 3. Polyhedral and ball-and-stick representations of the various building blocks (a), (b), (d), (e), (g), and (h) of compound **3** (c); ball-and-stick representation of five {Ni₄O₄} cubane cores (f) in compound **3**. WO₆, gray octahedra; PO₄, pink tetrahedra; VO₄, yellow tetrahedra; O, red or blue spheres; Ni, green sphere. (For interpretation of the references to colour in this figure legend, the reader is referred to the web version of this article.)

contains a {Ni₄O₄} cubane unit and the four nickel atoms are coordinated by one μ_4 -O from the central {PO₄} group of the *B*- α -{PW₉O₃₄} and three μ_3 -OH bridges. From another perspective, compound **2** can also be structurally described as a central {Ni₄(PO₄)₄} core (Fig. 2*i*) wrapped by two {(A- α -PW₉O₃₄)(NiOH)₃} units (Fig. 2*h*) and two {(B- α -PW₉O₃₄)(NiOH)₃} units (Fig. 2*j*). In the {Ni₄O₄} cubane unit of {Ni₄(PO₄)₄} core, the Ni-O distances are in the range 2.068(11)–2.137(10) Å and the Ni···Ni distances range from 3.080(10) to 3.194(10) Å. Bond valence sum (BVS) calculations indicated that all the Ni atoms are in the +2 oxidation state and W atoms are in the +6 oxidation state.

Compound **3** crystallizes in the monoclinic space group C2/c. Compound **3** (Fig. 3c) contains four lacunary *B*- α -{PW₉O₃₄} POM units (Fig. 3a) and one central {Ni₁₆(VO₄)₄(OH)₁₂} ({Ni16-3}) moiety (Fig. 3b). The whole {Ni16-3} cluster is well encapsulated and separated by four *B*- α -{PW₉O₃₄} units. The high-nuclearity {Ni16-3} cluster can be described as the condensation of four distorted {Ni₄O(OH)₃} cubane units connected by four {VO₄} linkers. There are five {Ni₄O₄} cubane units in all (Fig. 3h), creditable to the more active *B*- α -{PW₉O₃₄} unit. In the {Ni₄O₄} cubane unit, the Ni-O distances are in the range 2.066(14)–2.090(14) Å and the Ni···Ni distances range from 3.001(14) to 3.009(14) Å. In each {Ni₄O(OH)₃} cubane unit, the four nickel atoms are coordinated by one μ_4 -O from the central {PO₄} group of the *B*- α -{PW₉O₃₄} and three μ_3 -OH bridges. From another point of view, the structure of compound **3** can also be viewed as a tetramer comprising four tetra-nickel-substituted Keggin fragments ({Ni₄(OH)₃(B- α -PW₉O₃₄)}) (Fig. 3d) and four {VO₄} linkers (Fig. 3e). Alternatively, the structure of compound **3** can be regarded as a central {Ni₄(VO₄)₄} core (Fig. 3g) encapsulated by four {(B- α -PW₉O₃₄)(NiOH)₃} units (Fig. 3f) with idealized *Td* symmetry. BVS calculations showed that

all the nickel ions are in the +2 oxidation state, the vanadium ions are in the +5 oxidation state, and the tungsten ions are in the +6 oxidation state. It's noted that compound **3** is isostructural to the recently reported [{Ni₄(OH)₃AsO₄)₄(B- α -PW₉O₃₄)₄]²⁸⁻, where four {AsO₄} linkers occupy the positions of four {VO₄} linkers of **3** [30]. To our knowledge, using {VO₄} linker to build POMs is a difficult task compared with the commonly used {PO₄} and {AsO₄}, and no such POM has been reported prior to this work. Compound **3** represents currently the first POM-based nickel–vanadate cluster in POM chemistry, which not only provides a valuable molecular model for the nickel–vanadate catalysts with a well-defined structure but also pave a new way for design and synthesis of more efficient metal–vanadate water splitting catalysts in the near future.

2.2. Visible light-driven H₂ evolution catalyzed by **1–3**

The visible-light-driven H₂ evolution activities of compounds **1–3** were evaluated in a [Ir(ppy)₂(dtbbpy)]⁺/visible-light illumination/TEOA system. Hill and co-workers firstly used this system to explore new type of metal oxide-based HECs [29,30]. In this work, our study is mainly focused on the photocatalytic activity of these new compounds, leaving the optimization of this photocatalytic system aside. In this system, CH₃CN/DMF/H₂O solution was used owing to the solubility issues of photosensitizer [Ir(ppy)₂(dtbbpy)][PF₆] (ppy = 2-phenylpyridine; dtbbpy = 5,5'-di-tert-butyl-2,2'-bipyridine) in H₂O, triethanolamine (TEOA) as sacrificial electron donor and compounds **1–3** as the catalysts for H₂ evolution under visible-light illumination at 25 °C. Compounds **1–3** showed high activity for H₂ evolution after exposure to the white LED light, and no H₂ was detected in the dark. The

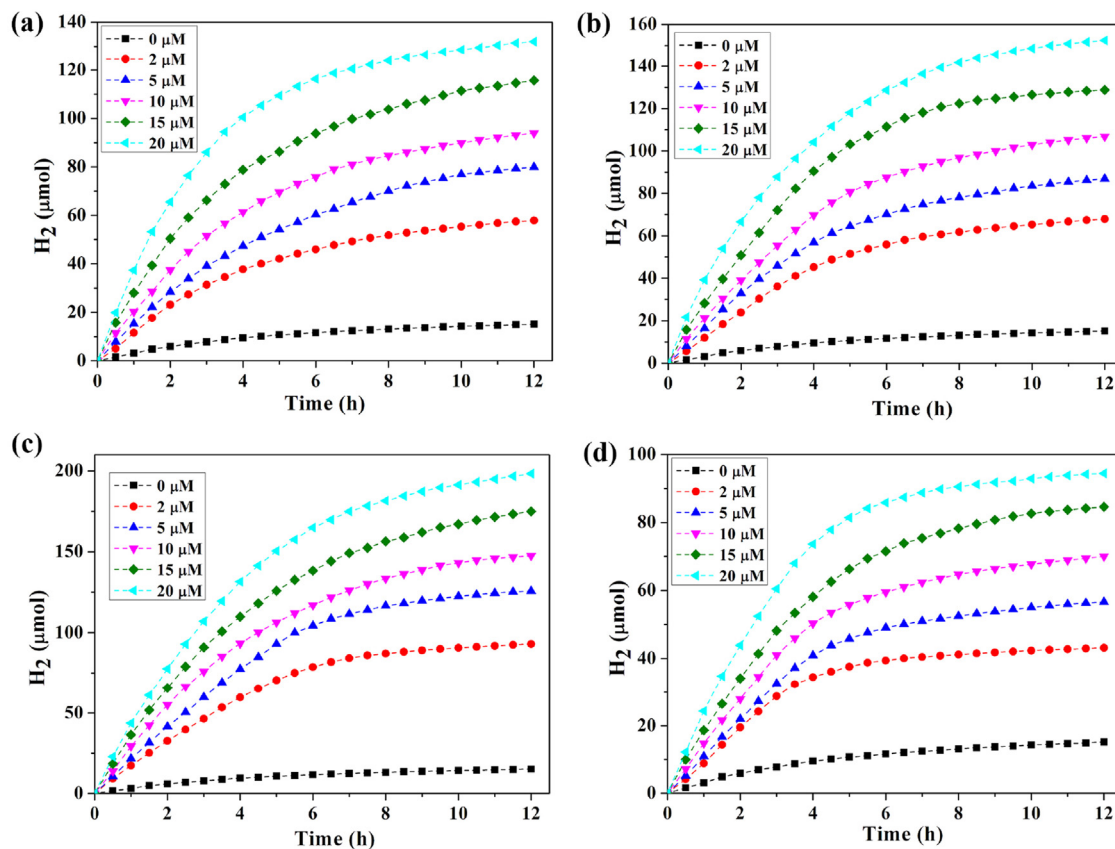


Fig. 4. Kinetics of H₂ evolution in the photocatalytic system at different concentrations of (a) **1**; (b) **2**; (c) **3** and [Ni₄(H₂O)₂(PW₉O₃₄)₂]¹⁰⁻.

H₂ evolution amount increased with time and a maximum value of 132.0 μmol, 152.5 μmol, and 198.3 μmol were achieved for 1.0 μmol of **1–3** (20 μM) after 12 h illumination (Table S2), respectively. The H₂ evolution amount obtained after 12 h of visible-light irradiation correspond to a high TON of 578.8, 679.1, and 931.1 for **1–3**, respectively (see Table S2 and Fig. S2). Accordingly, it was found that the photocatalytic activities of **1–3** follow the order of **1** < **2** < **3** (see Fig. 4 and Table S2). Moreover, the initial rate of photocatalytic H₂ evolution of the three reactions decreased over time. To explore the structure–performance relationship, we compared the structures of **1–3** and found that the number of the active {Ni₄O₄} cubane core is different in **1–3**. One, three, and five {Ni₄O₄} cubane cores correspond to **1**, **2**, and **3**, respectively. That is, the cubane increases in these three compounds follow the sequence: **1** < **2** < **3**. From this, we can see that the sequence of photocatalytic activity increases is in agreement with that of cubane number increases. Therefore, it can be concluded that catalytic performance is improved with increasing number of {Ni₄O₄} cubane. The H₂ yield increased with the catalyst concentrations increased and the TON decreased from 578.8 to 132.0 for **1**, from 679.1 to 152.5 for **2**, and from 931.1 to 198.3 for **3**, respectively, when the catalysts concentration increasing from 2 μM to 20 μM (Table S2 and Fig. S2). An initial turnover frequency (TOF_{initial} = n(H₂)/(n(catalyst) × 0.5 h)) in the first 0.5 h reached 100.5 h⁻¹, 112.7 h⁻¹, and 185.5 h⁻¹ for compounds **1**, **2**, and **3**, respectively (Fig. S3). The H₂ evolution rate at the end is quite low may be the photo-degradation of photosensitizer. Compound **3** represents currently the most active POM-based water splitting photocatalyst for H₂ evolution (Table S3).

Recently, Hill and co-workers studied the catalytic performance of [Ni₄(H₂O)₂(PW₉O₃₄)₂]¹⁰⁻ and it showed efficient photocatalytic H₂ evolution activity [29]. We carried out a control experiment using [Ni₄(H₂O)₂(PW₉O₃₄)₂]¹⁰⁻ under the same reaction

conditions applied for **1–3**. The photocatalytic H₂ evolution amount was achieved for 43.2 μmol and a high TON of 431.5 for 2 μM of [Ni₄(H₂O)₂(PW₉O₃₄)₂]¹⁰⁻ (Fig. 4d and Table S2). These results indicated that compounds **1–3** is more efficient than [Ni₄(H₂O)₂(PW₉O₃₄)₂]¹⁰⁻.

In addition, we have performed the control experiments only in the absence of **1–3** under the same experimental conditions. A maximum H₂ evolution amount of 15.19 μmol was evolved after 12 h photoirradiation (Fig. 4 black line), which corresponds too much less amount of H₂ evolution in the presence of **1–3**. This result suggests that compounds **1–3** are catalytically active and can effectively promote the H₂ evolution in the water splitting process. Furthermore, there was no H₂ evolution even in the presence of **1–3** without [Ir(ppy)₂(dtbbpy)][PF₆] or TEOA. Control experiments showed that [Ir(ppy)₂(dtbbpy)][PF₆], TEOA and catalysts **1–3** play crucial roles in H₂ evolution reactions. Without any one of the three species, negligible or no H₂ evolution can be detected.

In order to investigate the quenching mechanism of our photocatalytic system, the luminescence of photosensitizer [Ir(ppy)₂(dtbbpy)]⁺ has been measured in the presence of **1–3** or TEOA in N₂ deaerated CH₃CN/DMF/H₂O (11/33/4) solution (Fig. 5). The linear Stern–Volmer plot of the emission quenching data gives a KSV (10³ M⁻¹) of 5.12, 5.58, and 12.66 for oxidative quenching by compounds **1**, **2**, and **3**, respectively (Fig. S5). The Stern–Volmer analysis of the reductive quenching by TEOA yields a KSV of 13.22 × 10⁻³ (Fig. S5). Although the KSV of compounds **1–3** for oxidative quenching is about three orders of magnitude higher than that of TEOA for reductive quenching, the reductive process is still dominant given the much higher concentration of TEOA (0.3 M) relative to compounds **1–3** (20 μM). On the basis of the above experimental data, we propose the reaction mechanism in Scheme S1 for this

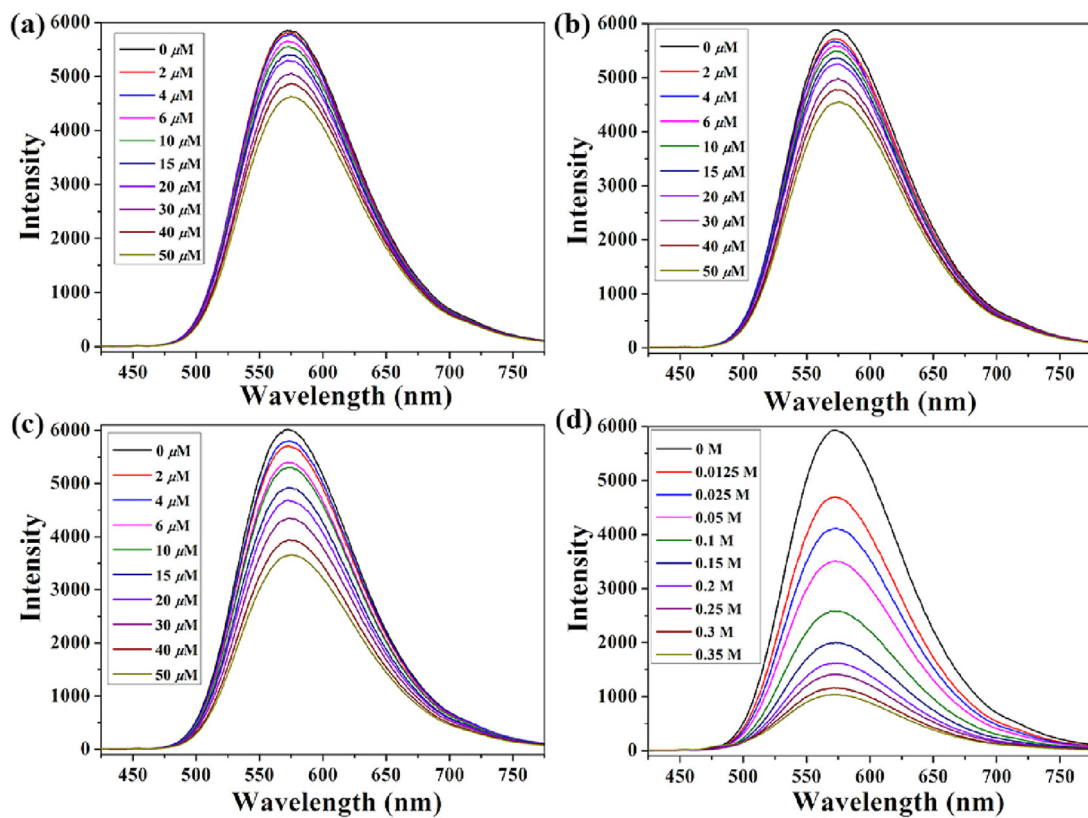


Fig. 5. Emission spectra of $[\text{Ir}(\text{ppy})_2(\text{dtbbpy})]^+$ (0.2 mM) as a function of added (a) **1**, (b) **2**, (c) **3**, and (d) TEOA.

visible-light-driven H_2 evolution. On the other hand, we also measured the luminescence of $[\text{Ir}(\text{ppy})_2(\text{dtbbpy})]^+$ in the presence of $[\text{Ni}_4(\text{H}_2\text{O})_2(\text{PW}_9\text{O}_{34})_2]^{10-}$ in N_2 deaerated $\text{CH}_3\text{CN}/\text{DMF}/\text{H}_2\text{O}$ (11/33/4) solution (Fig. S6). Stern–Volmer analysis gives a KSV of 4.91 for oxidative quenching by $[\text{Ni}_4(\text{H}_2\text{O})_2(\text{PW}_9\text{O}_{34})_2]^{10-}$ (Fig. S7). Accordingly, it was found that the KSV of $[\text{Ni}_4(\text{H}_2\text{O})_2(\text{PW}_9\text{O}_{34})_2]^{10-}$ and compounds **1–3** follow the order of $[\text{Ni}_4(\text{H}_2\text{O})_2(\text{PW}_9\text{O}_{34})_2]^{10-} < \mathbf{1} < \mathbf{2} < \mathbf{3}$, indicating that the quenching efficiencies between $\{\text{Ir}(\text{ppy})_2(\text{dtbbpy})\}$ and POMs might increase in the order of $[\text{Ni}_4(\text{H}_2\text{O})_2(\text{PW}_9\text{O}_{34})_2]^{10-} < \text{compound } \mathbf{1} < \text{compound } \mathbf{2} < \text{compound } \mathbf{3}$.

2.3. Reusability experiments of compounds **1–3**

The reusability experiment of compounds **1–3** was firstly carried out after the first run. As shown in Fig. S4 red line, after 12 h of irradiation, the H_2 evolution amount for the second run decreased to 85.5 μmol , 103.1 μmol and 127.7 μmol for **1–3**, respectively. Secondly, the reusability experiment of compounds **1–3** was performed after the second run. After 12 h of irradiation, the H_2 evolution amount for the second run decreased to 72.3 μmol , 92.1 μmol and 111.6 μmol for **1–3** (see Fig. S4 blue line), respectively. Thirdly, 0.5 mL H_2O , 0.25 mL TEOA, and 2.5×10^{-3} μmol $[\text{Ir}(\text{ppy})_2(\text{dtbbpy})]\text{[PF}_6]$ were added to the photocatalytic system after the third run. The H_2 evolution amount is slight higher than the first run (see Fig. S4, pink line) after 12 h of irradiation.

We also performed other reusability experiments of **1–3**. After the first run, 0.5 mL H_2O was added to the photocatalytic system for the second run. After 12 h of irradiation, the H_2 evolution amount was comparable to the red line of Fig. S4. Then, 0.25 mL TEOA was added to the reaction system for the third run. After 12 h of irradiation, the H_2 evolution amount was almost no change compared to the blue line of Fig. S4. Finally, 2.5×10^{-3} μmol

$[\text{Ir}(\text{ppy})_2(\text{dtbbpy})]\text{[PF}_6]$ was added to the photocatalytic reaction system after the third run. After 12 h of irradiation, the H_2 evolution amount was also comparable to the pink line of Fig. S4.

To further study the reusability of **1–3**, 2.5×10^{-3} μmol $[\text{Ir}(\text{ppy})_2(\text{dtbbpy})]\text{[PF}_6]$ was added to the photocatalytic reaction system after the first run and the H_2 evolution amount was just a little decrease compared to the first run after 12 h of irradiation. These results indicated $[\text{Ir}(\text{ppy})_2(\text{dtbbpy})]\text{[PF}_6]$ might be a dominant factor that influence the H_2 evolution activities.

2.4. Catalysts stability tests

Recently, the stability of molecular water splitting catalysts (WSCs) such as WOCs and HECs has received more and more concern as the WSCs might be unstable and decompose into catalytically active species. In this work, the stability of compounds **1–3** was tested by multiple experiments including DLS, UV-vis spectroscopy, catalysts aged experiments, and tetra-n-heptyl ammonium nitrate (THpANO_3) toluene extraction.

DLS measurements were performed after the photocatalytic H_2 evolution with 20 μM **1–3** and no nanoparticles can be detected after 12 h of irradiation (Figs. S8–S10). For comparison, we also carried out the DLS measurements using 15 μM $\text{Ni}(\text{NO}_3)_2 \cdot 6\text{H}_2\text{O}$ under the same reaction conditions applied for **1–3**. After 12 h of visible-light irradiation, the reaction solutions were conducted for DLS measurement and a diameter of 352.7 nm nanoparticles were readily detected (Fig. S11). These results indicated that compounds **1–3** themselves did serve as true molecular catalysts and did not decompose into Ni^{2+} (aq), nickel hydroxide or/and nickel oxide nanoparticles under the photocatalytic conditions.

UV-vis spectra of compounds **1–3** (1.0×10^{-4} M) were also carried out in the solution with different aging time (0–24 h). The UV-vis absorption spectra of **1–3** maintained unchanged during

a 24 h course of aging. This result indicated the stabilities of **1–3** during the photocatalytic H₂ evolution process (see Figs. S13–S15).

Moreover, THpANO₃ toluene extraction experiments were proved to be an effective method to quantitatively extract POMs from reaction solution and the remaining soluble species in aqueous solution could be easily quantified by elemental analysis as reported by Hill and co-workers [45]. Herein, we performed the experiments of THpANO₃ toluene extraction to detect the stability of compounds **1–3**. Firstly, after aging 20 μM of compounds **1–3** in the DMF/CH₃CN/TEOA/H₂O solution for 24 h, the solutions of compounds **1–3** were freeze-dried and dissolved in the 30 mL H₂O/toluene (v: v=1: 1) solution for THpANO₃ toluene extraction. Then, the remaining soluble species in the solutions were analyzed by inductively coupled plasma mass spectrometry (ICP-MS). A concentration of 0.47, 0.56 and 0.63 μM of Ni were detected for compounds **1–3**, respectively (Table S4), while the remaining W concentrations of 1.29, 1.25 and 1.44 μM for the corresponding solutions were detected, respectively. Secondly, the THpANO₃ toluene extraction experiments were also carried out after the photocatalytic H₂ evolution with 20 μM **1–3**. After 12 h of visible-light irradiation, the reaction solutions were extracted by the same technique and analyzed by ICP-MS. A concentration of 0.55, 0.53 and 0.76 μM of nickel remained in the reaction solution for compounds **1–3**, respectively. And, the detected W concentrations are 1.27, 1.24 and 1.51 μM for the corresponding solutions, respectively (Table S5). These THpANO₃ toluene extraction experiments and ICP-MS analysis results indicated that less than <0.24% of compounds **1–3** could have decomposed to Ni species in the photocatalytic H₂ evolution process. To eliminate that the dissociated Ni species could play an important role in the observed photocatalytic H₂ evolution activities of compounds **1–3**, we further performed the catalytic reactions with Ni(NO₃)₂·6H₂O under the same photocatalytic conditions applied for **1–3**. As shown in Fig. S12, both of the control Ni²⁺ ions showed much lower photocatalytic activities than compounds **1–3** (The H₂ evolution amount of control Ni²⁺ ions is <5.74% of that produced by **1–3**). The control experiments indicated that minimum Ni²⁺ ions cannot affect the overall photocatalytic performance of compounds **1–3**.

Finally, we also performed the visible-light-driven H₂ evolution reactions after compounds **1–3** aged for 12 h and 24 h. The photocatalytic H₂ evolution activities were almost the same as that of the fresh catalyst, respectively (Fig. S16). These experiments further proved that compounds **1–3** are stable under the visible-light-driven H₂ evolution process.

3. Conclusions

Three POM-based high-nuclear Ni clusters with varying number of {Ni₄O₄} cubane cores were synthesized. Compounds **1–3** are efficient catalysts for visible-light-driven H₂ evolution. Compound **3** represents the currently first nickel–vanadate cluster molecular HECs for H₂ evolution. Furthermore, the exploration of structure–performance relationship revealed that catalytic performance was improved with increasing number of {Ni₄O₄} cubanes. Multiple experiments including DLS, UV–vis absorption, catalysts aged experiments, and THpANO₃ toluene extraction confirmed that compounds **1–3** are structurally stable and act as the dominant active catalysts in the H₂ evolution system. In the field of POM-based HECs, the present research is an important milestone as it resolves three import problems: 1) determine the optimal TM element for cubane core from the perspective of efficiency-to-cost; 2) develop a reliable synthetic strategy for directional synthesis of TM cubane-containing POMs to achieve fine adjustment of the number of cubanes; 3) reveal the relationship between the number of cubanes and catalytic performance. Hence, it is believed that

this study will open a promising avenue for further design and synthesis of more efficient POM-based HECs in the near future. In continuation of our studies, we will probe into the impact of polymerization degree of POM shell on catalytic performance and the relevant study is ongoing in our group.

4. Experimental section

Materials and Methods. Reagent-grade chemicals were used as purchased without further purification. Na₉[A- α -PW₉O₃₄]·7H₂O and Na₈H[B- α -PW₉O₃₄] were synthesized according to the literature method [46]. Elemental analyses of Ni, V, P, W, K and Na were performed on a PLASMA-SPEC (I) inductively coupled plasma (ICP) atomic emission spectrometer. IR spectra were recorded on a Nicolet AVATAR FT-IR 330 Spectrophotometer with pressed KBr pellets. Thermogravimetric analyses were performed on a Perkin–Elmer TGA7 instrument in N₂ atmosphere with a heating rate of 5 °C min⁻¹. UV/Vis absorption spectra were measured by using a UV 2550 spectrophotometer (shimadzu, Japan). The emission spectra were recorded using the F-7000 FL spectrophotometer under 400 nm excitation. Dynamic light scattering (DLS) measurements were performed on a Zetasizer Nano 3600 instrument (Malvern Instrument Co.).

Synthesis of 1. NiCl₂·6H₂O (0.78 g, 3.26 mmol) and Na₉[A- α -PW₉O₃₄]·7H₂O (1.16 g, 0.40 mmol) were mixed in distilled water (40 mL). The mixture was vigorously stirred for 10 min and resulted in a light cloudy, green solution. Na₃PO₄·12H₂O (0.80 g, 2.1 mmol) was added and the pH of the mixture was maintained at 8.0–9.0 with 2.0 M NaOH (aq). The resulting green mixture was then stirred for 3 h at room temperature and a clear green solution was obtained by filtration. Addition of a 1.0 M KCl (0.5 mL) solution to the filtrate and stirred for another 20 min at room temperature. Green block crystals suitable for X-ray crystallography were obtained by slow evaporation at room temperature after about 10 days, quickly washed with cold distilled water, and air-dried to give 196 mg of **1**. Compound **1** can also be prepared according to the synthetic procedure put forward by Hill et. al [30]. Anal. Calcd (%) for **1**: Na, 4.78; K, 0.46; Ni, 7.37; P, 1.95; W, 51.93; Found: Na, 4.74; K, 0.45; Ni, 7.30; P, 1.93; W, 51.89. IR (KBr pellet) for **1**: $\tilde{\nu}$ =1114 (w), 1088 (w), 1056 (s), 1028 (s), 941 (s), 882 (m), 835 (s), 777 (w), 718 (s), 618 (w), 585 (w), and 513 cm⁻¹ (w).

Synthesis of 2. NiCl₂·6H₂O (0.5 g, 2.1 mmol) and Na₉[A- α -PW₉O₃₄]·7H₂O (1.0 g, 0.34 mmol) were mixed in distilled water (40 mL). The mixture was vigorously stirred for 10 min and obtained a clear, green solution. Then, CH₃COONa·3H₂O (0.60 g, 4.4 mmol) and Na₃PO₄·12H₂O (0.80 g, 2.1 mmol) were added to the above mixture and the pH was maintained at 8.0–9.0 with 2.0 M NaOH (aq). The resulting solution was heated to 100 °C for 3 h and a clear green solution was obtained by filtration. Green block crystals suitable for X-ray crystallography were obtained by slow evaporation at room temperature after about two weeks, quickly washed with cold distilled water, and dried in the air to give 186 mg of **2** (14.9% yield, based on tungstate). Anal. Calcd (%) for **2**: Na, 4.98; Ni, 7.26; P, 1.92; W, 51.23; Found: Na, 4.89; Ni, 7.14; P, 1.89; W, 51.19. IR (KBr pellet) for **2**: $\tilde{\nu}$ =1114 (s), 1091 (s), 1057 (s), 1028 (s), 939 (s), 884 (m), 836 (s), 777 (w), 725 (s), 620 (m), 584 (w), and 513 cm⁻¹ (w).

Synthesis of 3. NiCl₂·6H₂O (0.5 g, 2.1 mmol) and Na₈H[B- α -PW₉O₃₄] (1.0 g, 0.41 mmol) were mixed in distilled water (40 mL). The mixture was vigorously stirred for 10 min and formed a clear, green solution. Then, NaVO₃ (0.50 g, 4.1 mmol) was added, followed by adjusting the pH of the mixture at 8.0–9.0 with 2.0 M NaOH (aq). The mixture was heated to 100 °C for 3 h and a yellowish-green solution was obtained by filtration. Green block crystals suitable for X-ray crystallography were obtained by slow evaporation at room

temperature after about two weeks, quickly washed with cold distilled water, and air-dried to give 180 mg of **3** (14.0% yield, based on tungstate). Anal. Calcd (%) for **3**: Na, 5.15; Ni, 7.51; P, 0.99; V, 1.63; W, 53.0; Found: Na, 5.22; Ni, 7.63; P, 1.01; V, 1.67; W, 53.12. IR (KBr pellet) for **3**: $\tilde{\nu}$ = 1079 (m), 1029 (s), 955 (s), 937 (s), 891 (s), 800 (s), 733 (s), 620 (w), 586 (w), 508 (w), and 482 cm^{-1} (w).

Photocatalytic H₂ evolution Measurements. The H₂ evolution experiments were performed in a closed gas-circulating system CEL-SPH₂N (China Education Au-light Co., Ltd, Beijing) equipped with an external illumination Pyrex reaction vessel (total volume 100 mL) with a magnetic stirrer for vigorous stirring (1.0 \times 10³ rpm) and analyzed by using an automatic H₂ monitoring system. The vessel was filled with a solution containing a photosensitizer [Ir(ppy)₂(dtbbpy)][PF₆] (0.2 mM), a sacrificial electron donor TEOA (2 mL), CH₃CN (11 mL), DMF (33 mL), H₂O (4 mL) and different concentrations of catalysts **1–3** (0–20 μ M). Then, photosensitizer [Ir(ppy)₂(dtbbpy)][PF₆] (0.2 mM) was finally added quickly in last after putting all contents of reaction mixture and the system was evacuated in the dark to remove the air completely. The reaction was performed using a 100 W white LED light (400–780 nm). The produced H₂ was analyzed by a gas chromatography (GC7920) with a TCD and a 5 \AA molecular sieve column (2 m \times 3 mm) using N₂ as the carrier gas.

Acknowledgments

This work was supported by the National Natural Science Foundation of China (No. 21471027, 21671034), National Key Basic Research Program of China (No. 2013CB834802).

Appendix A. Supplementary data

Supplementary data associated with this article can be found, in the online version, at <http://dx.doi.org/10.1016/j.apcatb.2017.04.057>.

References

- [1] G. Li, Z. Lian, W. Wang, D. Zhang, H. Li, *Nano Energy* 19 (2015) 446–454.
- [2] X.C. Wang, K. Maeda, A. Thomas, K. Takanabe, G. Xin, J.M. Carlsson, K. Domen, M. Antonietti, *Nat. Mater.* 8 (2009) 76–80.
- [3] L. Yao, D. Wei, Y. Ni, D. Yan, C. Hu, *Nano Energy* 26 (2016) 248–256.
- [4] Z.J. Han, F. Qiu, R. Eisenberg, P.L. Holland, T.D. Krauss, *Science* 338 (2012) 1321–1324.
- [5] M. Wang, K. Han, S. Zhang, L.C. Sun, *Coord. Chem. Rev.* 287 (2015) 1–14.
- [6] M. Wen, Y. Kuwahara, K. Mori, D. Zhang, H. Lic, H. Yamashita, *J. Mater. Chem. A* 3 (2015) 14134–14141.
- [7] W.Y. Wang, J. Chen, C. Li, W.M. Tian, *Nat. Commun.* 5 (2014) 4647.
- [8] D. Zhang, P. Liu, S. Xiao, X. Qian, H. Zhang, M. Wen, Y. Kuwahara, K. Mori, H. Li, H. Yamashita, *Nanoscale* 8 (2016) 7749–7754.
- [9] X.-J. Kong, Z.K. Lin, Z.-M. Zhang, T. Zhang, W. Lin, *Angew. Chem. Int. Ed.* 55 (2016) 6411–6416.
- [10] G. Berggren, A. Adamska, C. Lambertz, T.R. Simmons, J. Esselborn, M. Atta, S. Gambarelli, J.-M. Mouesca, E. Reijerse, W. Lubitz, T. Happe, V. Artero, M. Fontecave, *Nature* 499 (2013) 66–69.
- [11] S.C. Lee, W. Lo, R.H. Holm, *Chem. Rev.* 114 (2014) 3579–3600.
- [12] H. Ogata, K. Nishikawa, W. Lubitz, *Nature* 520 (2014) 571–574.
- [13] M.W. Ribbe, Y. Hu, K.O. Hodgson, B. Hedman, *Chem. Rev.* 114 (2014) 4063–4080.
- [14] J.B. Broderick, B.R. Duffus, K.S. Duschene, E.M. Shepard, *Chem. Rev.* 114 (2014) 4229–4317.
- [15] C. Lydon, M.M. Sabi, M.D. Symes, D.-L. Long, M. Murrie, S. Yoshii, H. Nojiri, L. Cronin, *Chem. Commun.* 48 (2012) 9819–9821.
- [16] J.W. Zhang, Z.H. Liu, Y.C. Huang, J. Zhang, J. Hao, Y.G. Wei, *Chem. Commun.* 51 (2015) 9097–9100.
- [17] A. Bayaguid, J. Zhang, R.N.N. Khan, J. Hao, Y.G. Wei, *Chem. Commun.* 50 (2014) 13150–13152.
- [18] Y. Hou, M. Nyman, M.A. Rodriguez, *Angew. Chem. Int. Ed.* 50 (2011) 12514–12517.
- [19] T.M. Anderson, M.A. Rodriguez, F. Bonhomme, J.N. Bixler, T.M. Alam, M. Nyman, *Dalton Trans.* 40 (2007) 4517–4522.
- [20] M. Ibrahim, Y.H. Lan, B.S. Bassil, Y.X. Xiang, A. Suchopar, A.K. Powell, U. Kortz, *Angew. Chem. Int. Ed.* 50 (2011) 4708–4711.
- [21] X.-B. Han, Z.-M. Zhang, T. Zhang, Y.-G. Li, W. Lin, W. You, Z.-M. Su, E.-B. Wang, *J. Am. Chem. Soc.* 136 (2015) 5359–5366.
- [22] X.-B. Han, Y.-G. Li, Z.-M. Zhang, H.-Q. Tan, Y. Lu, E.-B. Wang, *J. Am. Chem. Soc.* 137 (2015) 5486–5493.
- [23] Z.J. Liang, D.D. Zhang, P.T. Ma, J.Y. Niu, J.P. Wang, *J. Chem. Eur.* 21 (2015) 8380–8383.
- [24] M. Ibrahim, A. Haider, Y. Xiang, B.S. Bassil, A.M. Carey, L. Rullik, G.B. Jameson, F. Doungmene, I.M. Mbomekalle, P.D. Oliveira, V. Mereacre, G.E. Kostakis, A.K. Powell, U. Kortz, *Inorg. Chem.* 54 (2015) 6136–6146.
- [25] A. Haider, M. Ibrahim, B.S. Bassil, A.M. Carey, A.N. Viet, X.L. Xing, W.W. Ayass, J.F. Miñambres, R.J. Liu, G.J. Zhang, B. Keita, V. Mereacre, A.K. Powell, K. Balinski, A.T. N'Diaye, K. Küpper, H.-Y. Chen, U. Stimming, U. Kortz, *Inorg. Chem.* 55 (2016) 2755–2764.
- [26] Y. Duan, J.M. Clemente-Juan, C. Giménez-Saiz, E. Coronado, *Inorg. Chem.* 55 (2016) 925–938.
- [27] Z.-J. Liu, X.-L. Wang, C. Qin, Z.-M. Zhang, Y.-G. Li, W.-L. Chen, E.-B. Wang, *Coord. Chem. Rev.* 313 (2015) 94–110.
- [28] H.J. Lv, J. Song, H.M. Zhu, Y.V. Geletii, J. Bacsa, C.C. Zhao, T.Q. Lian, D.G. Musaev, C.L. Hill, *J. Catal.* 307 (2013) 48–54.
- [29] H.J. Lv, W.W. Guo, K.F. Wu, Z.Y. Chen, J. Bacsa, D.G. Musaev, Y.V. Geletii, S.M. Lauinger, T.Q. Lian, C.L. Hill, *J. Am. Chem. Soc.* 136 (2014) 14015–14018.
- [30] H.J. Lv, Y.N. Chi, J.V. Leusen, P. Kögerler, Z.Y. Chen, J. Bacsa, Y.V. Geletii, W.W. Guo, T.Q. Lian, C.L. Hill, *Chem. – Eur. J.* 21 (2015) 17363–17370.
- [31] A. Ioannidis, E. Papaconstantinou, *Inorg. Chem.* 24 (1985) 439–441.
- [32] T. Yamase, X. Cao, S. Yazaki, *J. Mol. Catal. A: Chem.* 262 (2007) 119–127.
- [33] S.J. Li, S.M. Liu, S.X. Liu, Y.W. Liu, Q. Tang, Z. Shi, S.X. Ouyang, J.H. Ye, *J. Am. Chem. Soc.* 134 (2012) 19716–19721.
- [34] R.J. Liu, X.K. Shang, C.X. Li, X.L. Xing, X.L. Yu, G.J. Zhang, S.J. Zhang, H.B. Cao, L.H. Bi, *Int. J. Hydrogen Energy* 38 (2013) 9954–9960.
- [35] W.-C. Chen, C. Qin, X.-L. Wang, Y.-G. Li, H.-Y. Zang, Y.-Q. Jiao, P. Huang, K.-Z. Shao, Z.-M. Su, E.-B. Wang, *Chem. Commun.* 50 (2014) 13265–13267.
- [36] W.-C. Chen, C. Qin, Y.-G. Li, H.-Y. Zang, K.-Z. Shao, Z.-M. Su, E.-B. Wang, H.-S. Liu, *Chem. Commun.* 51 (2015) 2433–2436.
- [37] D.D. Zhang, C. Zhang, P.T. Ma, B.S. Bassil, R. Al-Oweini, U. Kortz, J.P. Wang, J.Y. Niu, *Inorg. Chem. Front.* 2 (2015) 254–262.
- [38] Y.-Q. Jiao, C. Qin, X.-L. Wang, F.-H. Liu, P. Huang, C.-G. Wang, K.-Z. Shao, Z.-M. Su, *Chem. Commun.* 50 (2014) 5961–5963.
- [39] X.Q. Du, J.L. Zhao, J.Q. Mi, Y. Ding, P.P. Zhou, B.C. Ma, J.W. Zhao, J. Song, *Nano Energy* 16 (2015) 247–255.
- [40] Y.-Q. Jiao, C. Qin, X.-L. Wang, C.-G. Wang, C.-Y. Sun, H.-N. Wang, K.-Z. Shao, Z.-M. Su, *Chem. Asian J.* 9 (2014) 470–478.
- [41] M.R. Gao, W.C. Sheng, Z.B. Zhuang, Q.R. Fang, S. Gu, J. Jiang, Y.S. Yan, *J. Am. Chem. Soc.* 136 (2014) 7077–7084.
- [42] V. Artero, M. Fontecave, *Coord. Chem. Rev.* 249 (2005) 1518–1535.
- [43] M.L. Helm, M.P. Stewart, R.M. Bullock, M.R. DuBois, D.L. DuBois, *Science* 333 (2011) 863–866.
- [44] P. Liu, J.A. Rodriguez, *J. Am. Chem. Soc.* 127 (2005) 14871–14878.
- [45] J.W. Vickers, H.J. Lv, J.M. Sumliner, G.B. Zhu, Z. Luo, D.G. Musaev, Y.V. Geletii, C.L. Hill, *J. Am. Chem. Soc.* 135 (2013) 14110–14140.
- [46] A.P. Ginsberg, *Inorg. Synth.* 27 (1990) 100.